metals

MDPI

Article

A New Method for Determining the Brittle-to-Ductile Transition Temperature of a TiAl Intermetallic

Sarper Nizamoglu *, Karl-Heinz Lang, Stefan Guth and Martin Heilmaier

Department of Mechanical Engineering, Institute for Applied Materials, Karlsruhe Institute of Technology, Engelbert-Arnold-Straße 4, 76131 Karlsruhe, Germany; karl-heinz.lang@kit.edu (K.-H.L.); stefan.guth@kit.edu (S.G.); martin.heilmaier@kit.edu (M.H.)

* Correspondence: sarper.nizamoglu@kit.edu; Tel.: +49-721-60847446

Received: 1 October 2020; Accepted: 18 November 2020; Published: 22 November 2020

Abstract: Intermetallic materials typically change their deformation behavior from brittle to ductile at a certain temperature called the Brittle-to-Ductile Transition Temperature (BDTT). This specific temperature can be determined by the Charpy impact, tensile or bending tests conducted at different temperatures and strain rates, which usually requires a large number of specimens. In order to reduce the number of necessary specimens for finding the BDTT, a new methodology comprising cyclic loadings as the crucial step was studied on a fully lamellar TiAl alloy with composition Ti-48Al-2Nb-0.7Cr-0.3Si. The loading blocks are applied isothermally under strain control and repeated on the same specimen at different temperatures. The development of plastic strain amplitude with increasing temperature is analyzed to determine the BDTT of the specimen. The BDTTs found with the described method agree well with literature data derived with conventional methods. With the loading strategy presented in this study, the BDTT and additionally the effect of strain rate on it can be found by using a single specimen.

Keywords: brittle-ductile transition temperature; fully lamellar TiAl intermetallic; cyclic loading; mechanical properties

1. Introduction

With an increasing temperature, many intermetallic alloys show a transition from brittle to ductile behavior. Brittle to Ductile Transition (BDT) can occur gradually with increasing temperature or within a very small temperature range of less than 100 °C. This transition has been observed in particular aluminides in Charpy impact tests [1], four-point bending tests [2,3] or tensile tests [4–9]. In Charpy impact tests, BDT is reflected by a significant increase of impact toughness and a change of the characteristic fracture surface from transcrystalline cleavage to ductile fracture [1]. Bending in the outer fibre before cracking in the four-point bending tests [2] and elongation in the tensile tests [4–9] increase remarkably beyond the BDT. In tensile tests, BDT is also connected with a remarkable decrease in the yield strength [6,7,9] and a change in the fracture mode from cleavage to intergranular fracture [4,8].

For materials that change their behavior from brittle to ductile in a limited temperature range, the Brittle-to-Ductile Transition Temperature (BDTT) can be defined. Until today, no uniform or standard definition of the BDTT has been established. Lin et al. and Noebe et al. used the results of tensile tests at different temperatures to define the BDTT [6,10]. Lin et al. determined the BDTT of a Ti-47Al-2Mn-2Nb alloy as the temperature, at which the elongation δ rises to 7.5%, and justified this definition by the fact that numerous dimples exist on the fracture surface beginning from this temperature [6]. Noebe et al. defined the BDTT of two NiAl alloys as the minimum temperature for which the materials show an elongation of ≥5% [10]. After Charpy impact tests at different temperatures on binary FeAl alloys, Herrmann et al. calculated the BDTT as the mean temperature in

the transition range between low and high impact energy values [1]. Based on results of the four-point bending tests at different temperatures on several FeAl intermetallics, Risanti et al. defined the BDTT as the mean value of the temperatures at which the material first reaches 1% and 3% of bending in the outer fibre [2]. In each study, at least three samples were used to determine the BDTT as the tests were carried out at different temperatures.

The BDTT of a material changes with its composition, microstructure, and loading rate. Risanti et al. studied the effect of Al content of Fe-Al alloys on the BDTT and found that the BDTT is increased significantly by increasing Al content in a binary Fe-Al alloy from 41.3 to 45 at% [2]. Lin et al. showed that with an addition of 1 at% B in the alloy TiAlMnNb, BDT is shifted to lower temperatures due to microstructure refinement [6]. For a two-phase TiAl alloy, the BDTT of a fully lamellar microstructure is higher than the BDTT of a duplex microstructure [7,9,11]. Results of tensile tests [5–7,10,11] and four-point bending tests [3] at different strain rates show that the BDT of several intermetallics is shifted to higher temperatures with an increasing strain rate. In order to determine the strain rate effect on BDTT, additional tests have to be conducted and more samples are necessary.

The purpose of this study is to present a new method for determining the BDTT of a TiAl intermetallic alloy, which requires only one specimen. The BDTTs at different deformation rates determined by this new method are compared with the literature data derived with conventional methods. By plotting the BDTTs at different strain rates in an Arrhenius plot the apparent activation energy for BDT is found.

2. Materials and Methods

The alloy used in this study, with a nominal composition of Ti-48Al-2Nb-0.7Cr-0.3Si (at%), was produced in ingot forms with a diameter of 24 mm and a length of 125 mm using the LEVICAST process [12]. The ingots were hot isostatically pressed in Ar atmosphere at 1150 °C/200 MPa for 4 h. The resulting microstructure is a fully lamellar structure with an average grain size of 358 µm and an average lath spacing of 1.55 µm [12], which is visualized in Figure 1. The ingots were then machined to cylindrical specimens with a gauge length of 17 mm and gauge diameter of 7 mm, on which the experiments were carried out.

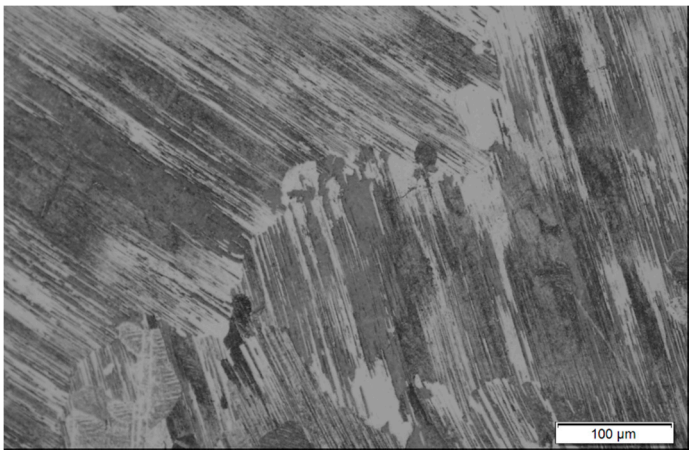

Figure 1. Optical micrograph of the material studied.

Three experiments referred to as A, B, and C with slightly different loading strategies were conducted. All experiments were carried out in laboratory air using a Schenck servo-hydraulic testing machine. Specimens were heated by an induction system. The geometry and the position of the induction coil were optimized until the axial temperature gradients within the gauge length did not exceed 2% of the nominal temperature. The temperature was measured by a band-thermocouple (type K) attached by a spring to the specimen surface in the center of the gauge length. The strain was

measured by a water-cooled extensometer, which was attached to the specimen within the gauge length. During each test, the specimen temperature, the stress and the strain signal were recorded continuously.

The input and output of experiment A are shown for two different temperature steps in Figure 2a. The whole experiment included nine incremental temperature steps of 50 °C starting at 500 °C. Each temperature step consisted of five cycles. A mechanical strain with an amplitude of $\varepsilon_a^{mech.} = 0.23\%$ and a strain ratio of $R_\varepsilon = \varepsilon_{min}/\varepsilon_{max} = -1$ were applied using a triangular wave shape at the strain rate of 0.46×10^{-4} s^{-1}. At the end of the fifth cycle, the control signal was switched from strain to force and the temperature of the specimen was increased from 500 to 550 °C after driving the force to zero. During the temperature increase, the residual force on the specimen was kept at zero level in order to avoid thermally induced stresses on the specimen. After the specimen had reached 550 °C, a 40 s dwell time at zero load was applied to reach thermal equilibrium. Then, the control signal was switched back to strain and the loading strategy was repeated at this temperature and the next seven temperature steps, which are given in Table 1. This experiment was used in order to study the BDTT of the material at a strain rate of 0.46×10^{-4} s^{-1} by using a single specimen.

Table 1. Temperature Steps of Each Experiment.

Experiment A and B	Experiment C
-	room temperature
-	100 °C
-	200 °C
-	300 °C
-	400 °C
500 °C	500 °C
550 °C	550 °C
600 °C	600 °C
650 °C	650 °C
700 °C	700 °C
750 °C	750 °C
800 °C	800 °C
850 °C	850 °C
900 °C	900 °C

Figure 2b provides the input and output of experiment B. This experiment included nine incremental temperature steps of 50 °C starting at 500 °C. The same load cycle of mechanical strain amplitude, ratio, and wave shape as in experiment A was applied for three cycles at a strain rate of 9.2×10^{-4} s^{-1}. At the end of the third cycle, the control signal was switched from strain to force and the residual force in the specimen was driven to zero in order to ensure equal initial stress conditions for the plastic deformation in the specimen. After that, the control signal was switched back to strain and three more triangular strain cycles with the same amplitude, but a strain rate of 1×10^{-4} s^{-1} were applied. Then, the control signal was switched back to force again, the remaining force was driven to zero and the temperature of the specimen was increased from 500 to 550 °C while keeping the force on the specimen at zero level. After a thermal equilibrium time of 40 s, this procedure was repeated for the temperature steps given in Table 1. The loading strategy in this experiment was used in order to study the BDTT of the material at two different strain rates of 9.2×10^{-4} s^{-1} and 1×10^{-4} s^{-1} by using only one specimen.

The input and output of experiment C at two different temperature steps are given in Figure 2c. This experiment included 14 incremental temperature steps starting at room temperature and ending at 900 °C. The same load cycle of mechanical strain amplitude, ratio, and wave shape as in experiments A and B was applied, this time at a different strain rate of 4.6×10^{-4} s^{-1}. At the end of the fifth cycle, the maximum or minimum mechanical strain was kept constant first in tension and then in compression, for 60 s of hold time, respectively. After the compression hold-time, the strain was driven to zero, the control signal was switched from strain to force and the temperature of the specimen

was increased from room temperature to 100 °C after driving the residual force to zero. During the temperature increase, the acting force was kept at zero level. When the temperature of the specimen reached 100 °C, a thermal equilibrium time of 40 s was allowed. Then, the control signal was changed to strain control and the loading strategy was repeated at this temperature and the next 14 temperature steps, which are given in Table 1. This experiment was used to study the effect of the load history on the BDTT.

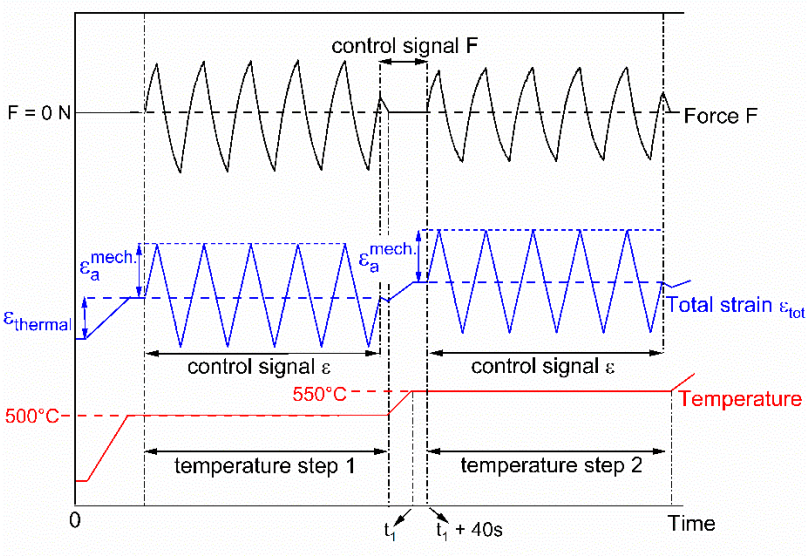

(**a**)

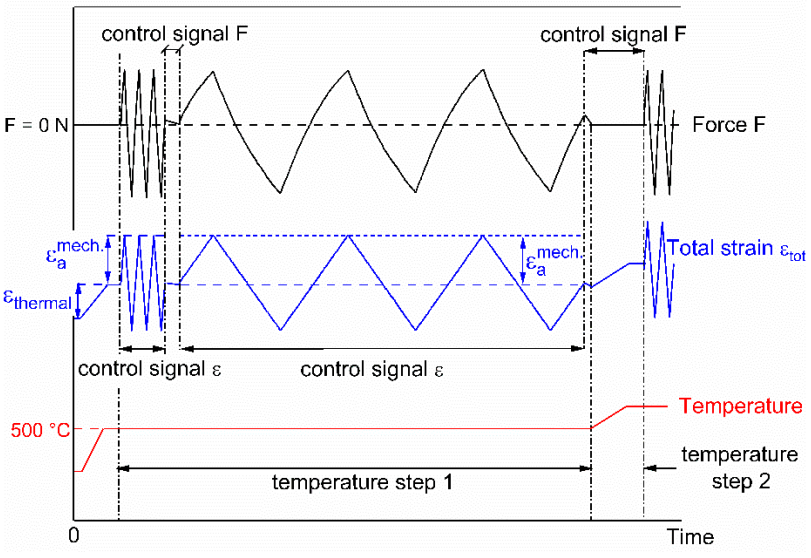

(**b**)

Figure 2. *Cont.*

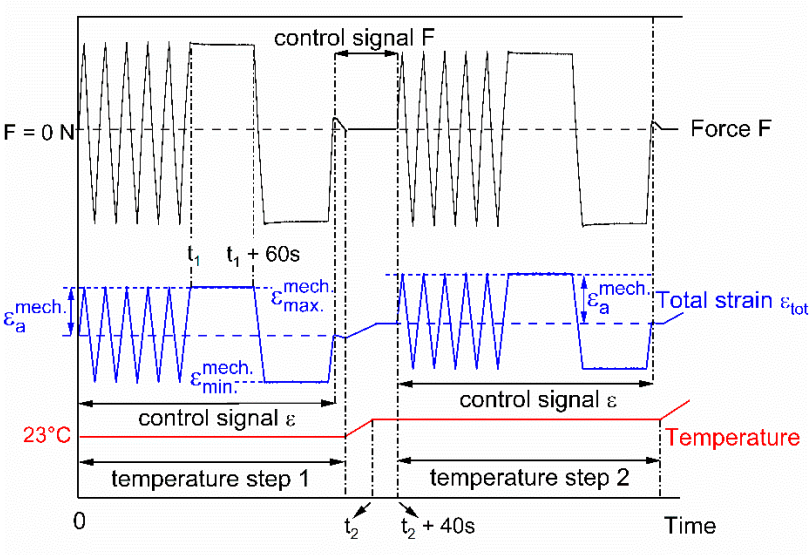

(**c**)

Figure 2. The loading strategies of (**a**) experiment A; (**b**) experiment B; (**c**) experiment C.

3. Results

From the recorded stress and strain signals, the plastic strain amplitude of each triangular cycle was determined as half of the width of the hysteresis at mean load. Figure 3 summarizes the results of all experiments conducted. The plastic strain amplitude as the mean value of the measurements at each temperature step was plotted versus the temperature. The change of plastic strain amplitude with temperature was divided into four temperature regimes: low temperature regime from room temperature up to 200 °C, moderate temperature regime from 200 up to 550 °C for the lower strain rates and up to 600 °C for the higher strain rates, high temperature regime range 1 and high temperature regime range 2, see Figure 3. In the low temperature regime up to 200 °C, the plastic strain amplitude increased with the increasing temperature, while in the moderate temperature regime, the material showed a negative temperature dependency of the plastic strain amplitude. This was followed by the first high temperature regime (range 1), in which the plastic strain amplitude increased again with temperature. In the second high temperature regime (range 2), the increase of plastic strain amplitude with temperature was greater than in range 1. Notice that the limiting temperatures for each regime depend on the strain rate: the first high temperature regime was between 600 and 750 °C for the two lower strain rates, while it was between 650 and 800 °C for both higher strain rates.

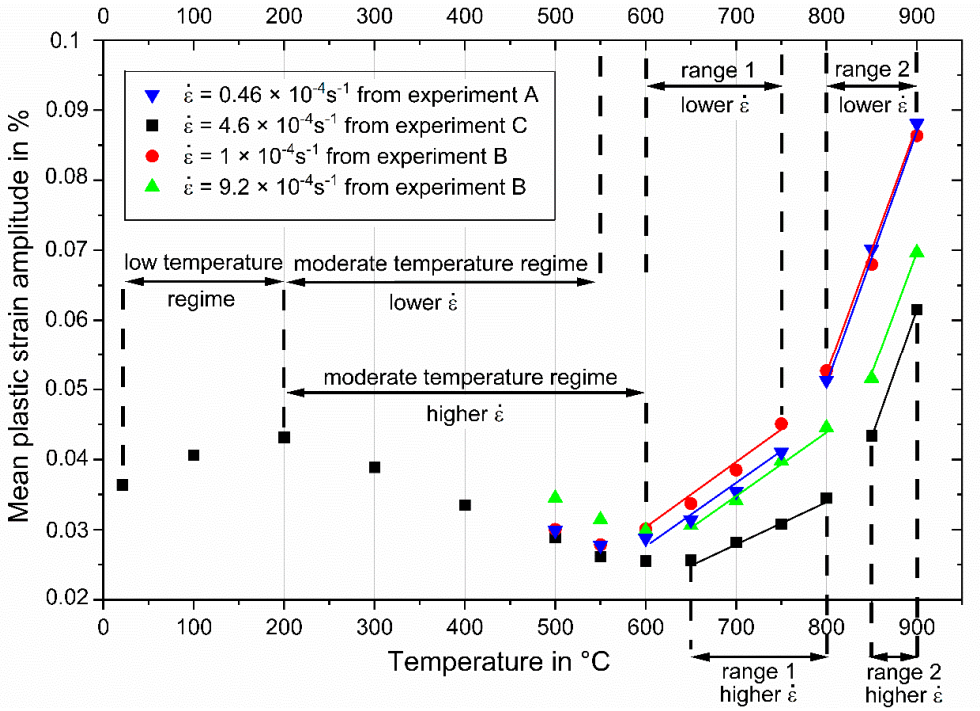

Figure 3. Relationship between the plastic strain amplitude from triangular cycles and the temperature at different strain rates.

4. Discussion

4.1. Mechanical Behavior of the Material in Different Temperature Regimes

Tensile test results on a lamellar Ti-47Al-2Cr-0.2Si alloy show that the flow stress decreases from room temperature to 200 °C [7] (p. 198). This can be explained by thermal activation of the acting deformation mechanisms in this temperature regime. In experiment C, we observe this phenomenon in the tested TiAl alloy, as the plastic strain amplitude at the strain rate of 4.6×10^{-4} s^{-1} increased slightly from room temperature to 200 °C, see Figure 3. In the moderate temperature regime, the plastic deformation decreased with increasing temperature. Tensile test results on Ti-47Al-1.5Nb-1Mn-1Cr-0.2Si-0.5B indicate that elongation decreased with increasing temperature near this temperature range; this behavior was explained with dynamic strain aging (DSA) effects [13]. Furthermore, several investigations on two phase TiAl intermetallic alloys showed a yield strength anomaly (YSA) in these alloys between 200 and 600 °C [14–16] with a peak depending on the composition and microstructure. After in situ straining observations of TiAl at temperatures between 200 and 400 °C Molénat et al. concluded that DSA promotes the Portevin-Le Chatellier effect in the temperature range of YSA [17]. DSA effects in TiAl alloys were also observed by Christoph et al. [18]. They suggested that Fe or B atoms interacting with dislocations could be the reason, as both are present in most of the technically relevant alloys [18]. The observed negative strain rate dependency at 500 °C in our experiments supports the idea of DSA. In the first cycle, the specimen deformed at the strain rate of 0.46×10^{-4} s^{-1} from experiment A showed higher stresses and a lower plastic deformation than the specimen deformed at the strain rate of 9.2×10^{-4} s^{-1} from experiment B, see Table 2. Hence, DSA effects may explain the decrease of plastic strain amplitude in the moderate temperature regime in our experiments.

Table 2. Comparison of the Results from the First Cycles at Different Strain Rates.

Temperature in °C	Strain Rate	Maximum Stress in MPa	Plastic Strain Amplitude in %
500	0.46×10^{-4} s^{-1}	268	0.034
500	9.2×10^{-4} s^{-1}	262	0.037

Beginning from range 1 of the high temperature regime, the plastic strain amplitude increased slightly with temperature. Consequently, DSA effects are not significant in this temperature range. The increase in plastic strain amplitude was steeper in temperature range 2 for each strain rate. Results of tensile tests with the same material at a strain rate of 1×10^{-4} s^{-1} show that the elongation changed significantly from 750 to 800 °C, see Figure 4. This indicates that BDT occurs within this temperature range. Results of our experiment at the same strain rate show that the increase of plastic deformation became more significant from 750 °C (range 1) to 800 °C (range 2), see the red circles in Figure 3. This suggests that the different slopes of the lines of the linear best fit in temperature ranges 1 and 2 are related to BDT. The different limiting temperatures for ranges 1 and 2 for the lower and higher strain rates are related to the strain rate dependence of the BDTT.

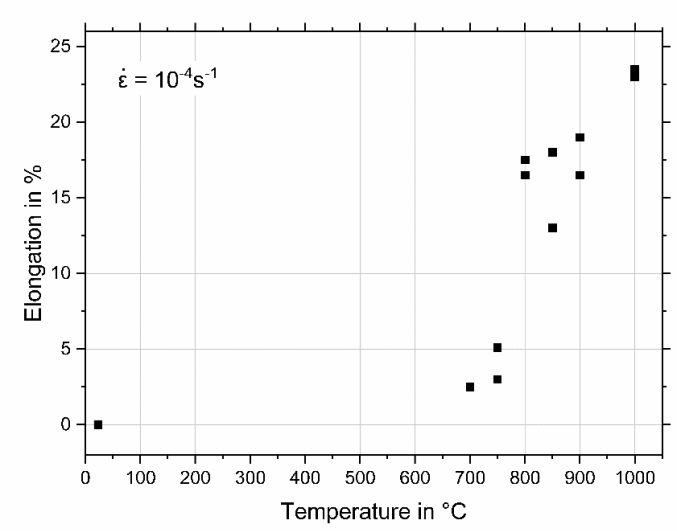

Figure 4. Elongation at fracture (full square symbols) obtained from tensile tests conducted on the same alloy as in this study, data from [12].

4.2. Determining the BDTT by a New Method

In order to determine the BDTT, the lines of the linear best fit of data in temperature ranges 1 and 2, respectively, were extended to find the point of intersection. The temperature at the intersection is then defined as the BDTT. In Figure 5a,b, this was done for the strain rates used in our experiments. Note that each point represents the plastic strain amplitude for the corresponding cycle. The resulting BDTTs are summarized in Table 3.

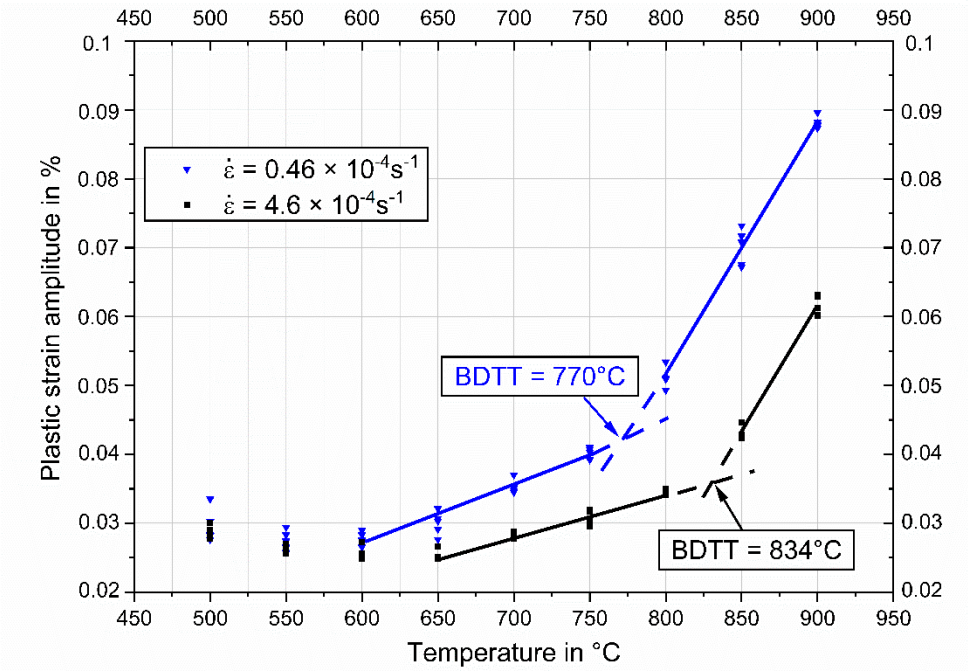

(**a**)

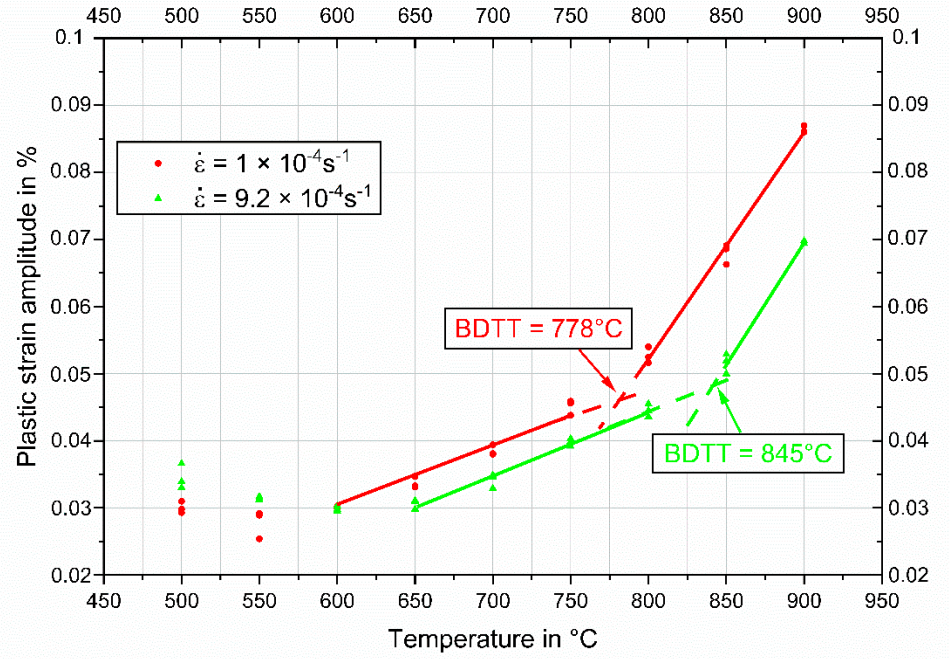

(**b**)

Figure 5. The resulting plastic strain amplitudes for different strain rates. (**a**) determination of BDTT at the strain rates of 0.46×10^{-4} s^{-1} and 4.6×10^{-4} s^{-1}; (**b**) determination of BDTT at the strain rates of 1×10^{-4} s^{-1} and 9.2×10^{-4} s^{-1}.

Table 3. BDTT of Ti-48Al-2Nb-0.7Cr-0.3Si Alloy at Different Strain Rates.

Strain Rate	BDTT
0.46×10^{-4} s^{-1}	770 °C
1×10^{-4} s^{-1}	778 °C
4.6×10^{-4} s^{-1}	834 °C
9.2×10^{-4} s^{-1}	845 °C

The BDTTs at different strain rates, which are determined by the presented method, were used to plot ln ($\dot{\varepsilon}$) against (BDTT × R)$^{-1}$ in Figure 6, where R is the ideal gas constant and an inverse linear relationship was found. For a thermally activated process, the apparent activation energy can be determined from the slope of the fit line, being 343 kJ/mol. This value is in the range of the activation energies of Ti diffusion in γ-TiAl phase (291 kJ/mol) [19] and Al diffusion in γ-TiAl phase (360 kJ/mol) [20], suggesting that BDT of this alloy is controlled by atomic diffusion mechanisms in γ-TiAl phase.

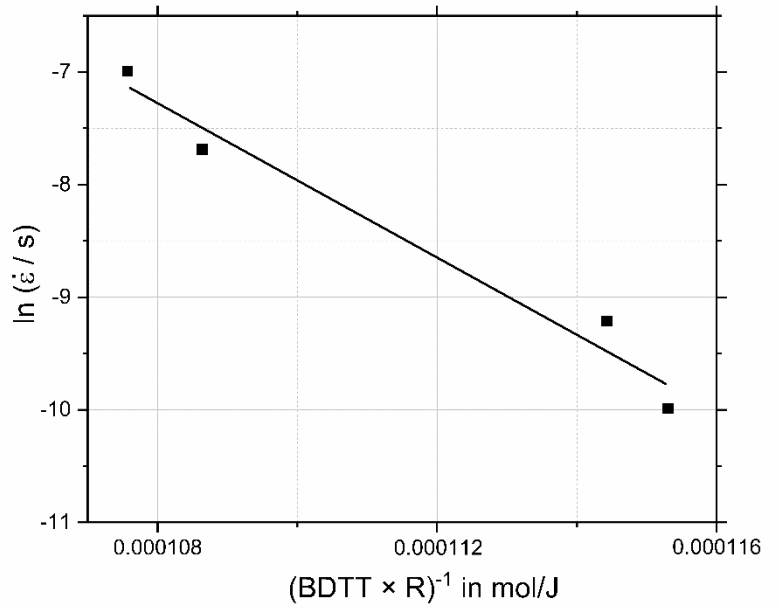

Figure 6. The linear relationship between ln ($\dot{\varepsilon}$) and (BDTT × R)$^{-1}$, full square symbols are experimental results from this study, the straight line is the linear best fit of data.

4.3. Effect of Different Load Strategies Used in This Study on the BDTT Determined by the New Method

Comparing the plastic strain amplitudes at different strain rates between 500 and 900 °C, it is noticeable that the plastic strain amplitudes at the strain rate of 4.6×10^{-4} s^{-1} are the lowest, see Figure 3. However, the different load histories of the experiments must be taken into account. The smaller values of the plastic strain amplitude at this strain rate are caused by a cyclic hardening of the material in the loading steps within the range between room temperature and 400 °C. In experiments A and B the specimens are not loaded in this temperature range, resulting in generally higher plastic strain amplitudes when compared to experiment C. Even at a temperature of 900 °C, the plastic strain amplitude for a strain rate of 4.6×10^{-4} s^{-1} in experiment C is lower than for a strain rate of 9.2×10^{-4} s^{-1} in experiment B. This indicates that the strain hardening due to plastic deformation in the low and moderate temperature regimes is effective up to high temperatures. Despite the cyclic hardening in the lower temperature stages in experiment C at 4.6×10^{-4} s^{-1}, the BDTT at this strain rate could be determined with the same new method as for the other strain rates.

The plastic strain amplitudes at each strain rate and temperature step reveal low scatter, see Figure 5a,b, with a maximal standard deviation of 0.003%. Note that five cycles were applied at 0.46

$\times 10^{-4}$ s^{-1} and 4.6×10^{-4} s^{-1} and three cycles were applied at 1×10^{-4} s^{-1} and 9.2×10^{-4} s^{-1}. Thus, for the investigated material, three to five cycles are sufficient to find the line of the linear best fit in the temperature ranges 1 and 2. However, for materials showing higher scatter of plastic strain amplitudes, more than five cycles might be recommended in order to have a statistically more accurate result. On the other hand, an increased cycle number at each temperature step means more accumulated plastic deformation, which may result in dislocation pileups and changes in dislocation structures that might in turn affect the BDTT. For that reason, a transmission electron microscopy analysis is recommended to study possible effects on dislocation structures when more cycles are to be repeated at each temperature step. In our experiments, due to the low number of repeated cycles and low plastic strain amplitudes resulting from each cycle, being below 0.055% at temperatures up to the first stage of ductile behavior, we did not expect pronounced dislocation pileups that could potentially affect the BDTT.

In our experiments, we used similar load strategies with small differences, e.g., different temperature steps (see Table 1) and a different amount of cycles (three triangular cycles or five triangular cycles followed by static loads). The differences in the load strategies do not seem to affect the BDTT, as these results correspond well with the literature data derived with tensile tests and four-point bending tests, see Table 4. Hence, each of the three load strategies together with the presented method in this study can be used to determine the BDTT of a material by using a single specimen. In order to find the effect of deformation rate on the BDTT, also by using a single specimen, we suggest the load strategy used in experiment B.

Table 4. BDTTs of TiAl Alloys for Different Strain Rates.

Material	Microstructure	Strain Rate in 10^{-4} s^{-1}	BDTT (°C)	BDTT Evaluation by	Reference
Ti-48Al-2Nb-0,7Cr-0.3Si	Fully lamellar	0.46–9.2	770–845	Method presented in this study	This study
Ti-48Al-2Nb-0,7Cr-0.3Si	Fully lamellar	1	750–800	Tensile tests, see Figure 4 in this study	[12]
TiAlMnNb	Nearly lamellar	0.1–100	750–1000	Tensile tests	[6]
TiAlMnNbB	Nearly lamellar	0.1–100	612–837	Tensile tests	[6]
Ti-46Al-3Nb-2Cr-0.2W	Fully lamellar	1–20	800–870	Tensile tests	[11]
Ti-46Al-3Nb-2Cr-0.2W	Duplex	1–20	700–780	Tensile tests	[11]
TiAl	L + segregated γ	1	800	Tensile tests	[7]
TiAl	-	-	700–800	Tensile tests	[8]
Ti-47Al-2Cr-2Nb-0.2B	Fully lamellar	5	800	Tensile tests	[21]
Ti-43.5Al-4Nb-1Mo-0.1B (TNM alloy)	Nearly lamellar γ	0.8	700–800	Tensile tests	[22]
Ti-44Al-4Nb-4V-0.3Mo-Y (novel β-γ TiAl alloy)	Nearly lamellar	1	800–850	Tensile tests	[23]
Ti-47Al-3Cr-3Nb	Duplex	-	700–800	Four-point bending tests	[24]

5. Conclusions

Three cyclic load strategies on single specimens have been employed to find the BDTT of a fully lamellar Ti-48Al-2Nb-0.7Cr-0.3Si alloy. The relationship between temperature and plastic strain amplitude, resulting from isothermally applied triangular cycles was analyzed to determine the BDTT. The results coincide well with conventionally measured BDTTs using multiple specimens from literature. An apparent BDT activation energy of the investigated alloy was measured as 343 kJ/mol, indicating that the BDT is controlled by diffusion mechanisms. Applying the loading strategy including two deformation rates and using the methodology presented in this paper, the BDTT of a material and the effect of strain rate on it can be calculated by using only one specimen.

Author Contributions: Conceptualization, S.N. and K.-H.L.; methodology, S.N.; investigation, S.N. and K.-H.L.; writing—original draft preparation, S.N.; writing—review and editing, K.-H.L., S.G. and M.H.; visualization, S.N.; supervision, M.H. All authors have read and agreed to the published version of the manuscript.

Funding: This research received no external funding.

Acknowledgments: We acknowledge financial support by the KIT-Publication Fund of the Karlsruhe Institute of Technology.

Conflicts of Interest: The authors declare no conflict of interest.

References

1. Herrmann, J.; Inden, G.; Sauthoff, G. Deformation behaviour of iron-rich iron-aluminium alloys at high temperatures. *Acta Mater.* **2003**, *51*, 3233–3242. [CrossRef]
2. Risanti, D.; Deges, J.; Falat, L.; Kobayashi, S.; Konrad, J.; Palm, M.; Pöter, B.; Schneider, A.; Stallybrass, C.; Stein, F. Dependence of the brittle-to-ductile transition temperature (BDTT) on the Al content of Fe-Al alloys. *Intermetallics* **2005**, *13*, 1337–1342. [CrossRef]
3. Booth, A.S.; Roberts, S.G. The brittle-ductile transition in γ-TiAl single crystals. *Acta Materialia* **1997**, *45*, 1045–1053. [CrossRef]
4. Kim, Y.-W. Intermetallic alloys based on gamma titanium aluminide. *JOM* **1989**, *41*, 24–30. [CrossRef]
5. Imayev, V.M.; Imayev, R.M.; Salishchev, G.A. On two stages of brittle-to-ductile transition in TiAl intermetallic. *Intermetallics* **2000**, *8*, 1–6. [CrossRef]
6. Lin, D.; Wang, Y.; Liu, J.; Law, C.C. The effects of temperature, strain rate and minor boron on tensile properties of wrought Ti-47Al-2Mn-2Nb alloy. *Intermetallics* **2000**, *8*, 549–558. [CrossRef]
7. Appel, F.; Wagner, R. Microstructure and deformation of two-phase γ-titanium aluminides. *Mater. Sci. Eng. R Rep.* **1998**, *22*, 187–268. [CrossRef]
8. Lipsitt, H.A.; Shechtman, D.; Schafrik, R.E. The deformation and fracture of TiAl at elevated temperatures. *Metall. Trans. A* **1975**, *6A*, 1991–1996. [CrossRef]
9. Kim, Y.-W.; Dimiduk, D.M. Progress in the understanding of gamma titanium aluminides. *JOM* **1991**, *43*, 40–47. [CrossRef]
10. Noebe, R.D.; Cullers, C.L.; Bowman, R.R. The effect of strain rate and temperature on the tensile properties of NiAl. *J. Mater. Res.* **1992**, *7*, 605–612. [CrossRef]
11. Kim, Y.-W.; Kim, S.-L. Effects of microstructure and C and Si additions on elevated temperature creep and fatigue of gamma TiAl alloys. *Intermetallics* **2014**, *53*, 92–101. [CrossRef]
12. Adilović, A. Untersuchung des Materialverhaltens von Titanaluminiden für den Einsatz im Abgasturbolader. Ph.D. Thesis, Karlsruhe Institute of Technology, Karlsruhe, Germany, 2016.
13. Fröbel, U.; Appel, F. Strain aging in γ(TiAl)-based and $\alpha_2(Ti_3Al)$ titanium aluminides. *Intermetallics* **2006**, *14*, 1187–1193. [CrossRef]
14. Morris, M.A. Dislocation configurations in two-phase Ti-Al alloys III. Mechanisms producing anomalous flow stress dependence on temperature. *Philos. Mag. A* **1994**, *69*, 129–150. [CrossRef]
15. Hashimoto, K.; Nobuki, M.; Tsujimoto, T.; Suzuki, T. Deformation behaviour of TiAl base alloy containing manganese at elevated temperatures. *ISIJ Int.* **1991**, *31*, 1154–1160. [CrossRef]
16. Umakoshi, Y.; Nakano, T. Plastic behaviour of TiAl crystals containing a single set of lamellae at high temperatures. *ISIJ Int.* **1992**, *32*, 1339–1347. [CrossRef]
17. Molénat, G.; Couret, A.; Caillard, D. Peierls friction stresses and dynamic strain ageing in TiAl and Fe-30at.% Al alloys. *Mater. Sci. Eng. A* **1997**, *234–236*, 600–663. [CrossRef]
18. Christoph, U.; Appel, F.; Wagner, R. Dislocation dynamics in carbon-doped titanium aluminide alloys. *Mater. Sci. Eng. A* **1997**, *239*, 39–45. [CrossRef]
19. Kroll, S.; Mehrer, H.; Stolwijk, N.; Rosenkranz, R.; Frommeyer, G. Titanium self-diffusion in the intermetallic compound γ-TiAl. *Zeitschrift fuer Metallkunde* **1992**, *83*, 591–595. [CrossRef]
20. Herzig, C.; Przeorski, T.; Mishin, Y. Self-diffusion in γ-TiAl: An empirical study and atomistic calculations. *Intermetallics* **1999**, *7*, 389–404. [CrossRef]
21. Chan, K.S.; Shih, D.S. Fatigue and fracture behavior of a fine-grained lamellar TiAl alloy. *Metall. Mater. Trans. A* **1997**, *28A*, 79–90. [CrossRef]

22. Schwaighofer, E.; Clemens, H.; Mayer, S.; Lindemann, J.; Klose, J.; Smarsly, W.; Güther, V. Microstructural design and mechanical properties of a cast and heat-treated intermetallic multi-phase γ-TiAl based alloy. *Intermetallics* **2014**, *44*, 128–140. [CrossRef]
23. Zhang, S.Z.; Zhao, Y.B.; Zhang, C.J.; Han, J.C.; Sun, M.J.; Xu, M. The microstructure, mechanical properties, and oxidation behavior of beta-gamma TiAl alloy with excellent hot workability. *Mater. Sci. Eng. A* **2017**, *700*, 366–373. [CrossRef]
24. Brotzu, A.; Felli, F.; Marra, F.; Pilone, D.; Pulci, G. Mechanical properties of a TiAl-based alloy at room and high temperatures. *Mater. Sci. Technol.* **2018**, *34*, 1847–1853. [CrossRef]